Evaluation of climate effect on resilient modulus of granular subgrade material

Tianshu Lin [a], Tatsuya Ishikawa [b,*], Jiaqiang Yang [a], Tetsuya Tokoro [c]

[a] Graduate School of Engineering, Hokkaido University, Kita 13, Nishi 8, Kita-Ku, Sapporo 060-8628, Japan

[b] Faculty of Engineering, Hokkaido University, Kita 13, Nishi 8, Kita-Ku, Sapporo 060-8628, Japan

[c] Faculty of Engineering, Hokkai-Gakuen University, 1-1, Minami 26 Nishi 11, Chuo-ku, Sapporo 064-0926, Japan

Keywords

Resilient modulus, Unsaturated soil, Freeze-thaw action, Subgrade material, Laboratory element test

Abstract

This study examines the effects of freeze-thaw actions and the concurrent seasonal fluctuations in water content, named as climate effect in this study, on the resilient modulus of subgrade materials to evaluate their mechanical behavior in cold regions. A series of suction-controlled resilient modulus tests on subgrade materials with variant freeze-thaw, wheel loads, and water contents conditions were conducted using a newly developed test apparatus. Test results were used to construct a simple model to estimate the climate effect on the resilient modulus by considering the synergistic effects between water content and freeze-thaw. Besides, this study calculated the fatigue life of eight local flexible pavement projects with variant subgrade layer moduli considering climate effect by combining the newly proposed model and long-term in-situ measured data. Results proved that climate-related degradation of the subgrade materials decreases the fatigue life of asphalt pavements in cold regions.

1. Introduction

* Corresponding author. Email address: t-ishika@eng.hokudai.ac.jp

In snowy cold regions such as Hokkaido, a northern island in Japan, pavement structures suffer annually freeze-thaw cycles as the 0°C isotherm may penetrate deep into the pavement. Freeze-thaw action deteriorates pavement structures in two ways as frost-heave and thaw-weakening. The swelling of soil during freezing conditions caused by an increasing presence of ice lens finally leads to cracking in the asphalt-mixture layer (hereafter referred to as the "As layer"). Thaw-weakening means a drop of base and subgrade layer strength and stiffness caused by suddenly rising water content, which comes from the inflow of snowmelt water or the thawing of ice lenses, and deteriorates uniformity of particle skeleton structure after freeze-thaw action (Jong et al., 1998; Simonsen and Isacsson, 1999).

A detailed understanding of the mechanical behavior of the base/subgrade materials during freeze-thaw is essential to develop a mathematical model of the mechanical response of the base/subgrade layer in cold regions and incorporate it into the theoretical design method for pavement structures. To achieve such understanding, it is necessary to quantitatively capture the deformation-strength characteristics of unbound granular base course and subgrade materials subjected to cyclic freeze-thaw actions under various compaction conditions and water contents through laboratory element tests with high-precision under sufficiently controlled experimental conditions. As the result, a significant loss of stiffness from frozen to thawed and an increase in the recovery period are observed in both in-situ bearing capacity test for frozen and thawed pavement structure and laboratory element test for frozen, thawed, and recovered base/subgrade material (Berg et al., 1996; Cole et al., 1981; Johnson et al., 1978; Simonsen et al., 2002; Simonsen and Isacsson, 2001). However, partly due to the apparatus limitation and different research topics, the synergistic effects between water content and freeze-thaw on the resilient modulus (M_r), which is the key factor of base/subgrade layer as it associates with the elastic modulus (E) used in the design calculation for pavement structures applying the multi-layer elastic theory or finite element method, have not yet been quantitatively evaluated and modeled in these tests. In this study, the synergistic effects between freeze-thaw actions and concurrent seasonal fluctuations in water content, named as climate effect, will be examined.

Ishikawa et al. (2019a) examine the climate effect on the resilient deformation characteristics of base course materials through a series of resilient modulus tests on base course materials under various water contents. As a complementary and further research, this study examines and evaluates the climate effect

on M_r of subgrade material through a series of suction-controlled resilient modulus tests (hereafter referred to as the "MR test") with variant freeze-thaw, wheel loads, and water contents conditions. This study names the unsaturated condition and freeze-thaw action applied in the MR test as climate process. Besides, this study attempts to develop a simple mathematical model of the mechanical response of subgrade materials subjected to climate effect, in order to establish a method for evaluating the long-term performance of the granular subgrade layer at pavement structures in cold regions.

2. Conventional Models

2.1 Universal model and Ng model

Mechanistic-Empirical Pavement Design Guide (MEPDG) (AASHTO, 2008) proposed a universal model to predict the resilient modulus with stress variables as shown in Eq. (1).

$$M_r = k_1 p_a \left(\frac{\theta}{p_a}\right)^{k_2} \left(\frac{\tau_{oct}}{p_a} + 1\right)^{k_3} \quad (1)$$

where k_1, k_2, k_3 are regression constants; p_a is atmospheric pressure and set as 101 kPa in this study; θ is bulk stress (kPa); τ_{oct} is octahedral stress (kPa).

However, this model cannot reflect the effect of moisture content. To overcome this shortcoming, several models (Cary and Zapata, 2011; Liang et al., 2008; Ng et al., 2013) are proposed based on the universal model. Within these models, the Ng model shown in Eq. (2) adds an independent stress state variable that incorporates matric suction effects. It shows good applicability on predicting resilient modulus of unsaturated unbound granular materials through the relatively higher coefficient of determination (R^2) value than other models (Han and Vanapalli, 2016).

$$M_r = k_1 p_a \left(\frac{\theta}{p_a}\right)^{k_2} \left(\frac{\tau_{oct}}{p_a} + 1\right)^{k_3} \left(\frac{\psi}{\sigma_{net}} + 1\right)^{k_4} \quad (2)$$

where k_1, k_2, k_3, k_4 are regression constants; p_a is atmospheric pressure; θ is bulk stress; τ_{oct} is octahedral stress; σ_{net} is net mean stress (kPa), defined as [θ /3-u_a]; ψ is matric suction (kPa).

2.2 Enhanced Integrated Climatic Model

MEPDG also suggests a model, named as EICM (Enhanced Integrated Climatic Model) (NCHRP, 2004), to capture the freeze-thaw effect on M_r as shown in Eq. (3). This model adds a new factor,

F_{env}, on the universal model (Eq. (1)) to represent the reduction of M_r due to freeze-thaw. F_{env} is a reduction factor defined by the ratio of M_r for freeze-thawed soil divided by M_r for unfrozen soil.

$$M_r = F_{env} \cdot k_1 p_a \left(\frac{\theta}{p_a}\right)^{k_2} \left(\frac{\tau_{oct}}{p_a} + 1\right)^{k_3} \quad (3)$$

3. Test Apparatus and Material

3.1 Freeze-thaw triaxial apparatus

Fig. 1 illustrates the schematic diagram of the apparatus used in this study, which consists of a cyclic triaxial test apparatus that can apply cyclic axial loads, and three low-temperature baths which could circulate low-temperature fluids (antifreeze) in the cap, pedestal, and inner cell to control the temperature separately. The size of the specimen is 170 mm in height and 70 mm in diameter. The apparatus can apply the matric suction (ψ) by controlling pore-water pressure (u_w) from the pedestal end and pore-air pressure (u_a) from the cap end (Fig. 1 (b) and (c)). Details about the test apparatus could be found in the previous study (Lin et al., 2019a).

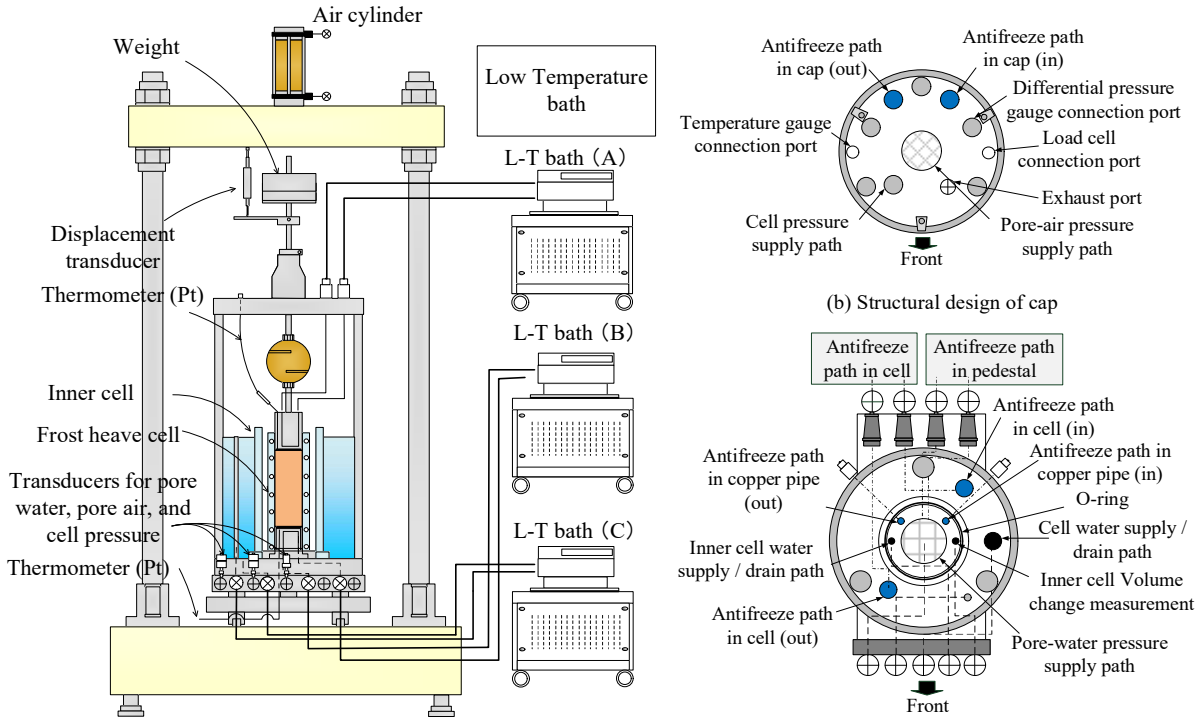

(a) Schematic diagram of test apparatus

(b) Structural design of cap

(c) Structural design of pedestal

Fig. 1. Freeze-thaw triaxial apparatus.

3.2 Toyoura sand

Toyoura sand is a type of Japanese standard sand, employed as the test material in this study and laboratory element tests by many other researchers. As a non-frost-susceptible material, it is classified as a poorly graded sand (SP) according to ASTM classification. Specimens were prepared by air pluviation method and the degree of compaction is 96% and dry density (ρ_d) is 1.58 g/cm^3 to satisfy the pavement subgrade layer standard provided by Japanese Ministry of Land, Infrastructure, Transport and Tourism (Japan Road Association, 2006).

Fig. 2 shows the soil-water characteristic curve (SWCC) of Toyoura sand obtained from this apparatus (Lin et al., 2019b). The SWCC of this soil is S-shaped with an inflection point where the matric suction increased as the volumetric water content decreased, and the shape qualitatively matches the results of previous studies (Ishikawa et al., 2014). Besides, the difference in SWCCs between a freeze-thawed specimen and an unfrozen specimen can hardly be recognized. This phenomenon is originated in no particle breakage due to freeze-thaw action, which led to little change in the water retentivity and permeability before and after freeze-thawing (Ishikawa et al. (2016)). The fitting curve for unfrozen specimen through Fredlund and Xing model (1994) is also displayed in the figure.

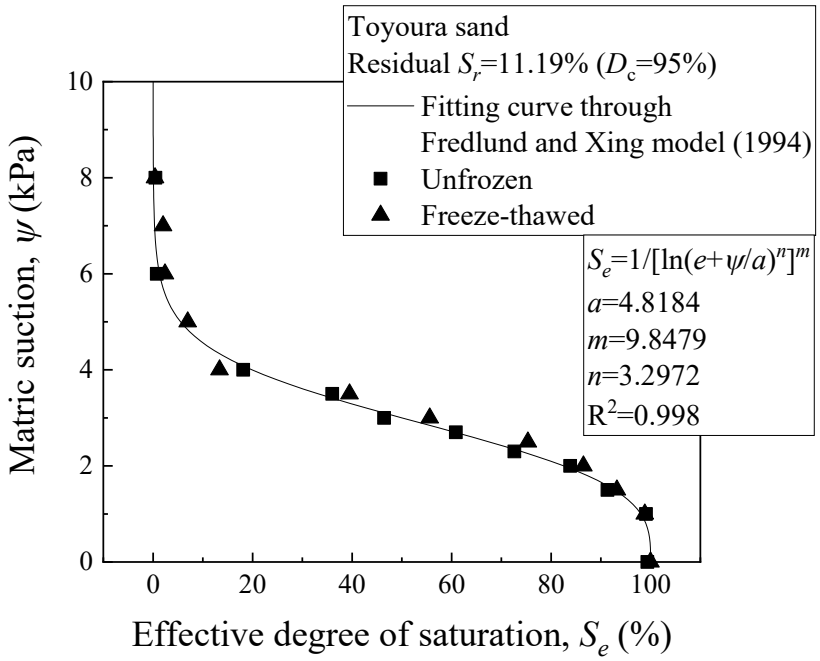

Fig. 2. Soil-water characteristic curves of Toyoura sand (after Lin et al., 2019b).

4. Laboratory Testing Program

4.1 MR test

Resilient modulus is especially important in mechanistic pavement design procedure and considerable researches had been conducted since Seed et al. (1955) proposed the concept of resilient modulus as the ratio of the amplitude of cyclic deviator stress to the amplitude of the resultant recoverable axial strain. In this study, MR test is performed according to AASHTO test standard T307-99 (AASHTO, 2003). Due to the limitation of the apparatus, this study applied a loading pulse with a frequency of 0.2 Hz (Fig.3 (a)), which is different from the AASHTO standard haversine-shaped loading pulse with a frequency of 10 Hz (Fig.3 (b)). According to the measured loading data, it is recognized that haversine-shaped load was almost reproduced though the frequency is much lower than the recommended value in AASHTO standard. Examination of this limited loading frequency would be discussed in the latter part.

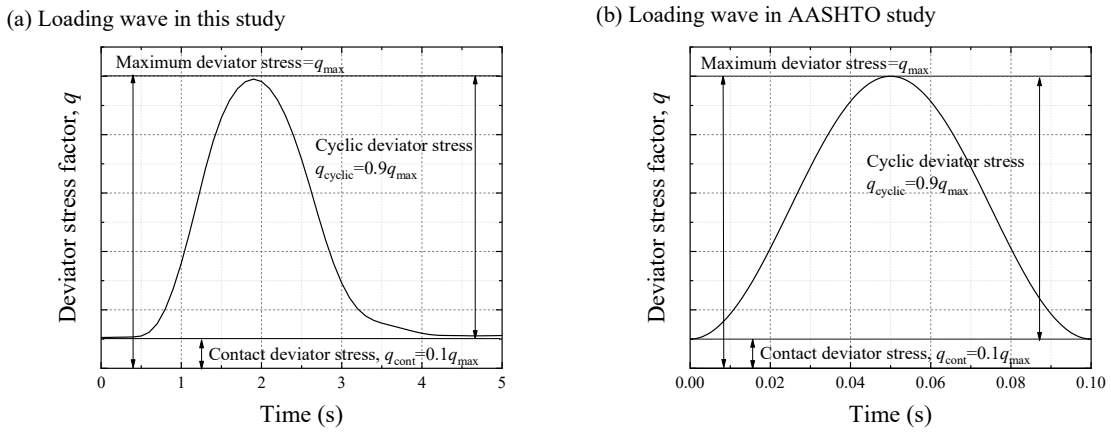

Fig. 3. Loading wave in (a) this study, (b) AASHTO standard.

AASHTO standard has 11 loading steps from MR-0 to MR-10. According to the AASHTO standard, MR-0 aims to make sure the cap completely reaches the top end of the specimen. For this reason, this study prolonged the loading number from 1000 cycles to 2000 cycles to ensure a stable residual strain after MR-0. Besides, the vertical stress in stages MR-4, 5, 9, and 10 are significantly larger than the stress measured at the actual situation in Japan (Kishikawa et al., 2017). The overstress in MR-4, 5 increased the relative density, and the results of MR- 6, 7, 8 cannot be evaluated accurately (Aoki et al., 2018). To sustain the relative density, this study skipped MR-4, 5, 9, and 10 and inserted MR-1.5, 2.5,

6.5, and 7.5 to keep the total test step as 11. Table 1 lists details of applied stress, like confining pressure (σ_c), maximum deviator stress (q_{max}), constant deviator stress to keep positive contact between the cap and the specimen (q_{cont}), cyclic deviator stress (q_{cyclic}), and the loading number (N_c). Fig. 3 illustrates the definitions of q_{max}, q_{cont}, and q_{cyclic} in one loading cycle. In the MR tests, water can freely drain in or out during the loading process due to the test standard T307-99 (AASHTO, 2003). Within past studies, some undrained resilient modulus tests were conducted under saturated conditions (Guo et al., 2013; Lin et al., 2019). The buildup of pore-water pressure was overestimated as the in-situ base/subgrade layer rarely to be saturated. Some other undrained resilient modulus tests for unsaturated specimens did not use a suction-controlled method to prepare specimen (Chen et al., 2018; Fall et al., 1997; Khoury and Zaman, 2004; Yang et al., 2005) and the precise suction value during the test could not be measured. Based on the axis-translation technique, a suction-controlled undrained resilient modulus test method is proposed for saturated and unsaturated specimen (Cary and Zapata, 2016; Yang et al., 2008). However, an undrained condition is still not fully reproduced in these laboratory element tests as the water path is closed during loading while the pore-air pressure path is open to control it as a constant to keep a constant effective confining pressure, named as Constant Water content (CW) test (Fredlund and Rahardjo, 1993). A Consolidated Undrained (CU) resilient modulus test for unsaturated specimens with controlled suction still lacks investigation. Therefore, this study only focuses on the drained condition. It is noted that the pore water in the subgrades shall be excited under traffic loading and it may take a long time to dissipate. Hence, subgrade layers under traffic loading are likely under undrained conditions. The buildup of pore-water pressure during cyclic loading in undrained conditions seriously deteriorates the mechanical properties and engineering performance of subgrade material. A suction-controlled consolidated undrained MR test method is under investigation to improve the understanding of how pore-water pressure develops under cyclic loading.

Table 1. Loading conditions of MR tests.

Name	σ_c (kPa)	q_{max} (kPa)	q_{cont} (kPa)	q_{cyclic} (kPa)	N_c
MR-0	41.4	27.6	2.76	24.84	2000
MR-1	41.4	13.8	1.38	12.42	100

MR-1.5	41.4	20.7	2.07	18.63	100
MR-2	41.4	27.6	2.76	24.84	100
MR-2.5	41.4	34.5	3.45	31.05	100
MR-3	41.4	41.4	4.14	37.26	100
MR-6	27.6	13.8	1.38	12.42	100
MR-6.5	27.6	20.7	2.07	18.63	100
MR-7	27.6	27.6	2.76	24.84	100
MR-7.5	27.6	34.5	3.45	31.05	100
MR-8	27.6	41.4	4.14	37.26	100

4.2 Test sequence

This study designed five types of MR test named as Unfrozen test (hereafter referred to as the "U test"), Unfrozen-Wheel loads test (hereafter referred to as the "UW test"), Freeze-Thaw test (hereafter referred to as the "FT test"), Freeze-Thaw-Wheel loads test (hereafter referred to as the "FTW test"), and Freeze-Wheel loads-Thaw test (hereafter referred to as the "FWT test"). Each test was conducted under saturated and unsaturated conditions. U tests measure M_r of subgrade material at unfrozen status which simulates normal season. UW tests condition aims to simulate subgrade material suffered wheel loads at the normal season. FT tests, by applying one-dimensional freeze-thaw action on specimen before MR test, aim to detect the resilient modulus just after freeze-thaw action. FTW tests, by applying an additional wheel loads process after freeze-thaw action, could simulate a subgrade material that suffered wheel loads at thawing season. FWT tests, by applying additional wheel loads process between freeze-thaw action, could simulate a subgrade material suffered wheel loads at the freezing season. All tests start with a fully saturated specimen, by confirming the pore pressure coefficient is 0.96 or more. In this study, a fully saturated specimen for test under saturated condition is prepared as follows: (1) Supplying CO_2 to replace the air in the specimen. (2) Supplying de-aired water through the specimen. As this study uses the filter method and axis translation technique to prepare an unsaturated specimen from a saturated condition, CO_2 could not be supplied in the specimen. The saturation process for test under unsaturated conditions is prepared as follows: (1) Supplying de-aired water through the specimen. (2) Applying back

pressure of 200 kPa step by step. The u_w, u_a, and σ_c are 200, 200, and 220 kPa at the end. Table 2 summarizes the sequence of each test. For example, the most complicated test, FWT test in unsaturated condition, is performed as follows: (1) Applying consolidation process. Within this process, predetermined consolidation stress of 41.4 kPa, which is the same as the highest confining pressure in the MR test (AASHTO, 2003), is applied to the specimen. The u_w, u_a, and σ_c are set as 200, 200, and 241.4 kPa according to the 200 kPa back pressure. (2) Applying suction process to obtain an unsaturated specimen. This process is carried out by decreasing u_w while keeping u_a and σ_c constant. (3) Applying freezing process by lowering specimen temperature. (4) Applying wheel loads process with predetermined cyclic deviator stress. (5) Applying thawing process by raising specimen temperature. (6) Performing MR test. More details like test technique for unsaturated specimen preparation, stress state during wheel loads process, and temperature conditions applied during the freeze-thaw process are explained in the next section. It is noted that suction process is applied prior to freezing process in FT, FTW, and FWT tests under unsaturated conditions as shown in Table 2. This sequence means matric suction is under control during the whole freeze-thaw action, which involves a high level of experimental skill. Another simpler test sequence applies freeze-thaw action on a saturated specimen and controls matric suction after freeze-thaw action, which is far from the actual situation as the subgrade layer hardly to be saturated in winter. Lin et al. (2019b) compared performance of specimens prepared by these two test sequences and found that more water drains out and axial displacement is larger during the freeze-thaw process when freeze-thaw action is applied on a saturated specimen. Consequently, this study applied suction process prior to freezing process as it better reproduces the actual situation that subgrade material meets during the freezing season.

Table 2. Test sequence for U, UW, FT, FTW, and FWT test.

Test name	Test sequence													
	Consolidation process		Suction process		Freezing process		Wheel loads process		Thawing process		Wheel loads process		MR test	
U	→	○	→	○/×	→	×	→	×	→	×	→	×	→	○
UW	→	○	→	○/×	→	×	→	×	→	×	→	○	→	○

FT	→	○	→	○/×	→	○	→	×	→	○	→	×	→	○
FTW	→	○	→	○/×	→	○	→	×	→	○	→	○	→	○
FWT	→	○	→	○/×	→	○	→	○	→	○	→	×	→	○

Note: ○means Applied this progress; × means Skipped this progress.

4.3 Climate and wheel loading conditions

4.3.1 Suction process

As mentioned in the Introduction part, to examine and evaluate the climate effect on M_r of subgrade material, a series of suction-controlled MR tests with two kinds of water content, saturated and unsaturated, under variant freeze-thaw history and wheel loads condition are performed. The unsaturated specimen used in this study has a 40% degree of saturation, equals to 16% volumetric water content, as the long-term field measurement data (Ishikawa et al., 2012) of the volumetric water content of a subgrade layer in Hokkaido is about 16%. According to SWCC of Toyoura sand (Fig. 2), the matric suction (ψ) is set as 3.75 kPa by axis translation technique (Fredlund and Morgenstern, 1977) to obtain this unsaturated specimen. Suction process starts from the fully saturated and isotropic consolidated condition by decreasing pore-water pressure in steps while keeping both confining pressure and pore-air pressure constant. A decrease of pore-water pressure means an increase of matric suction, which causes the drainage of pore-water from the specimen. Upon attaining an equilibrium condition, the drainage is stopped. The above-described procedure is then repeated for a higher value of matric suction, ψ, until 3.75 kPa to finally obtain an unsaturated specimen. It is noted that, stress condition in Table 1 is used in the saturated condition, based on a total stress approach in which the triaxial system measures the mechanical response of the material subjected to different combinations of cyclic deviator stress (q_{cyclic}) and confining pressures (σ_c). From the unsaturated soil mechanics perspective, the air phase becomes important in the measurement and control of matric suction and the total stress is replaced by the net normal stress (Cary and Zapata, 2011), which is the difference between the total stress and the pore-air pressure (σ-u_a). By using the axis translation technique, the confining pressure becomes the net confining pressure (σ_c- u_a) and the axial stress, σ_a, becomes the net axial stress (σ_a- u_a). This approach does not affect the way the deviator stress is defined since the air pressure will affect σ_a and σ_c in the same

proportion. Consequently, the stress value in Table 1 is the same for an unsaturated test when the confining pressure becomes the net confining pressure.

4.3.2 Freezing and thawing process

Temperatures of cap and pedestal during freeze-thaw process are shown in Fig. 4. One-dimensional freeze-thaw action is achieved in the following steps. The initial temperature of cap and pedestal were set and kept to 0 ℃ and 16.8 ℃ respectively and a frost heave cell (see Fig. 1) is mounted to restrict the radial deformation during freeze-thaw process. The thermal shock is applied at the top end of the specimen prior to freezing to avoid supercooling. Then, temperatures of cap and pedestal are lowered to -18.9 ℃ and -2.1 ℃ respectively with a constant cooling rate of 1.67 ℃/hr. Similar to the previous research (Aoki et al., 2018), a constant cooling rate of 1.67 ℃/hr is used in this study to avoid the supercooled state, caused by too large rates, or excessive test time, caused by too small rates. Next, temperatures of cap and pedestal are kept for 5 hours to ensure the uniformity of unfrozen water. The thawed status is achieved by raising temperatures of cap and pedestal to 5 ℃ and 16.8 ℃ with a heating rate of 1.67 ℃/hr. Open-system freeze-thaw process is used in this test by opening the pedestal water plumbing path during the freeze-thaw process, which means the specimen could drain in or out water freely. Referring to JGS 0172-2009 (Japanese Geotechnical Society, 2009), applied axial stress during the freeze-thaw process is set as 10 kPa. More details of freeze-thaw action and specimen performance like drainage volume and axial displacement could be found in previous research (Lin et al., 2019b).

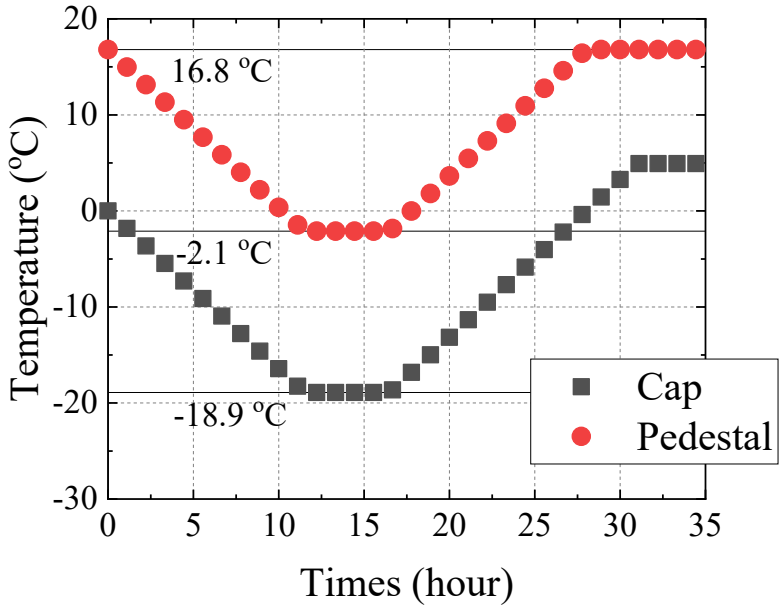

Fig. 4. Temperature of cap and pedestal during freeze-thaw process.

4.3.3 Wheel loads process

The wheel loads in this study could be classified into three types: loads on the unfrozen specimen (UW test), loads on the frozen specimen (FWT test), and loads on the thawed specimen (FTW test). Loading cycles of wheel loads in UW, FTW, and FWT tests are 1000 times. Loading frequency and pulse shape are the same as those in MR test loading (Fig. 3 (a)). Constant deviator stress (q_{cont}) and cyclic deviator stress (q_{cyclic}) during wheel loads process should be determined through an appropriate method to simulate actual stress state of the subgrade layer during normal or freezing seasons. General Analysis of Multi-layered Elastic Systems (GAMES) (Maina and Matsui, 2004) is used to determine the q_{cont} and q_{cyclic} on the subgrade layer caused by a 49-kN wheel load on a typical pavement structure in the Japanese design guide. Fig. 5 illustrates the pavement structure and parameters like Young's modulus, E, and Poisson's ratio, v, used in this study. These values come from the Japanese design guide recommended value (Japan Road Association, 2006). It is noted that these moduli are roughly estimated values, which may have a large difference with in-situ measured data. Besides, the design guide sets moduli of base, subbase, and subgrade layers as constant, which implies a necessity of modification. A modification with variant E caused by climate effect will be realized and introduced in the latter part. According to GAMES calculation results, the q_{cont} and q_{cyclic} of wheel loads process in UW and FTW,

252 which simulate wheel loads in normal and thawing season, are set as 9.6 and 26.2 kPa. The q_{cont} and
253 q_{cyclic} of wheel loads process in FWT, which simulate wheel loads in freezing season, are set as 9.6 and
254 24.5 kPa. In FWT test, removing frost heave cell before applying wheel loads process is necessary as it
255 restricts the specimen in a radial direction. Then, a copper pipe, which could circulate antifreeze, is
256 installed around the specimen to keep the frozen status during the whole wheel loads process. When the
257 wheel loads process is finished, the copper pipe is removed, and the thawing period is started.

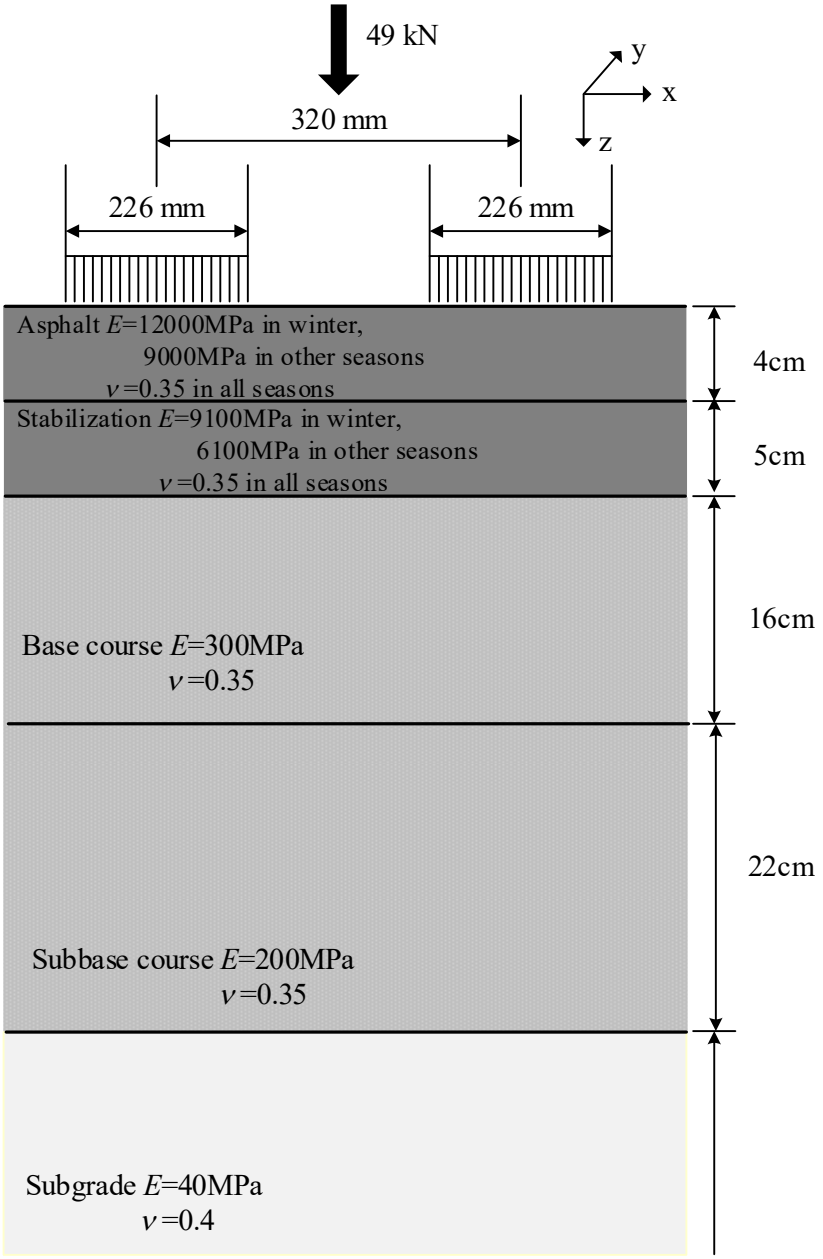

258

259 Fig. 5. Pavement structure and E, ν used in GAMES.

5. Test Results and Discussions

5.1 Effects of loading frequency

Examining the influence of loading frequency is necessary to check the reliability of test results, and the usefulness and generality of the proposed testing method, as the loading frequency used in AASHTO standard is 10 Hz. Toyoura sand specimens with three water content (40%, 70%, and 100% degree of saturation, matric suction for such degree of saturation is 3.75kPa, 3 kPa, and 0 kPa respectively) are prepared to perform MR test with two different apparatus, freeze-thaw triaxial apparatus and medium-size triaxial apparatus. Medium-size triaxial apparatus could apply loading frequencies of 10 Hz. Details of medium-size triaxial apparatus could be checked in previous research (Ishikawa et al., 2014). Fig. 6 plots the average resilient modulus ratio between M_r of MR-1 to MR-8 with high frequency and low frequency under different matric suction conditions. The fitting curve shown in Fig. 6 is obtained through Eqs. (5) and (6) and will be explained later. First of all, all ratios are higher than 1, which means that higher loading frequency always leads to a higher modulus regardless of the degree of saturation. Fig. 6 also illustrates that matric suction influences the average resilient modulus ratio between different loading frequencies. To be precise, the average resilient modulus ratio increases with ψ, which also implies that the frequency effect is more significant for a specimen with higher matric suction.

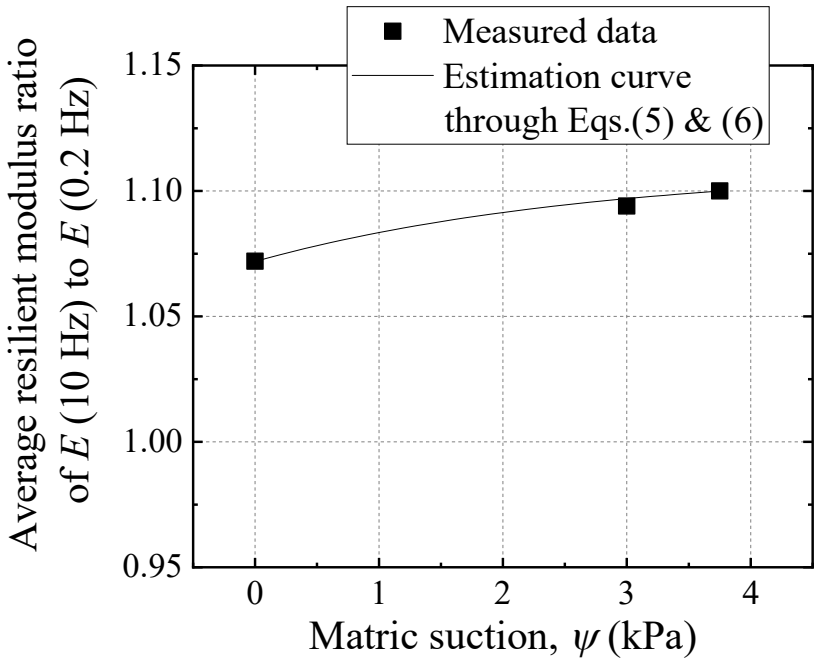

Fig. 6. Average resilient modulus ratio under different matric suction conditions.

Eq. (4) was proposed to quantitively describe the frequency effect on the resilient modulus (Kim et al., 1997).

$$\frac{E(f)}{E(0.5\ Hz)} = 1 + F(\psi) * Log(f) \quad (4)$$

where f is loading frequency; $E(0.5\ Hz)$ is resilient modulus obtained at f=0.5 Hz; $E(f)$ is predicted resilient modulus at any frequency, f; $F(\psi)$ is referred as the frequency effect, which is affected by matric suction, ψ.

Based on Eq. (4), the average resilient modulus ratio between 10 Hz and 0.2 Hz could be expressed as follows:

$$\frac{E(10\ Hz)}{E(0.2\ Hz)} = \frac{\frac{E(10\ Hz)}{E(0.5\ Hz)}}{\frac{E(0.2\ Hz)}{E(0.5\ Hz)}} = \frac{1+F(\psi)*Log(10)}{1+F(\psi)*Log(0.2)} = \frac{1+F(\psi)}{1-0.6989F(\psi)} \quad (5)$$

Based on Eq. (5) and measured average resilient modulus ratio, the value of $F(\psi)$ under three matric suction values could be determined as shown in Fig. 7.

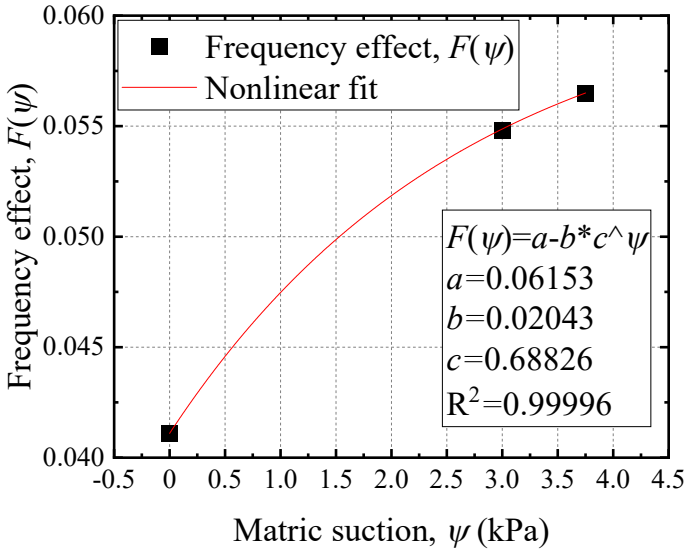

Fig. 7. Frequency effect under different matric suction conditions.

A nonlinear equation ($F(\psi)$=a-b*c^ψ) is chosen as the fitting model because it would not meet such question that $F(\psi)$ increases to an unrealistic level when the ψ is extremely large. Besides, parameters in this nonlinear equation have a clearer physical meaning. When ψ goes to an infinite value or zero, $F(\psi)$ equals to a or a-b. As a result, a means upper limit of $F(\psi)$ and a-b means $F(\psi)$ when the specimen

is fully saturated. Substituting fitted frequency effect, $F(\psi)$, into Eq. (5), predicted average resilient modulus ratio with high accuracy could be obtained (see the black line in Fig. 6).

Consequently, M_r obtained through freeze-thaw triaxial apparatus with limited loading frequency could be converted to general AASHTO standard M_r through Eqs. (5) and (6). Since limited unsaturated condition and soil type are used to investigate the effect of loading frequency, this conversion should only be used here to overcome frequency effect. Besides, different loading frequencies may lead to some unclear changes in pore water pressure, pore air pressure, and so on. More study on the frequency effect is necessary to improve understanding of resilient modulus.

$$F(\psi) = 0.06153 - 0.02043 * 0.68826^{\psi} \quad (6)$$

5.2 Effects of matric suction on resilient modulus

Aiming to quantitively analyze the effect of stress state, freeze-thaw action, matric suction on the M_r, this study performs regression analysis with Ng model to obtain the value of k_1, k_2, k_3, k_4 from a series of MR tests and investigate how freeze-thaw action and fluctuating water content affect these values. Figs. 8 to 12 illustrate M_r of U, UW, FT, FTW, and FWT test respectively. The red dot is measured M_r and the fitting surface is obtained through Ng model (Eq. (2)). It is noted that these results are converted data through Eqs. (5) and (6) and seen as general AASHTO standard resilient modulus. Table 3 lists regression analysis results through Ng model. Regression analysis here is performed regardless of the degree of saturation. In other words, saturated and unsaturated U tests are treated as one group to perform regression analysis. UW, FT, FTW, and FWT tests are regression analyzed in the same method. High R^2 values validate the applicability of Ng model.

It is well known that M_r highly relates to stress variables. To be specific, M_r increases with lower deviator stress (q) or higher confining pressure (σ_c) and matric suction (ψ). This is because a higher σ_c leads to increasing of frictional force, which helps resist soil deformation. This trend could be found during all test results as shown in Fig. 6 to 10. As shown in Figs. 8 to 12, all unsaturated tests have a higher M_r than saturated tests regardless of freeze-thaw and wheel loads history. Additionally, M_r obtained from unsaturated specimen through all tests has a more slanting surface, in other words, q and σ_c have a more significant influence on the M_r when the specimen is unsaturated. Consequently, suddenly rising water

content, induced by the inflow of snowmelt water and the thawing of ice lenses at thawing season or heavy rainfall at summertime, greatly degrades the subgrade layer stiffness.

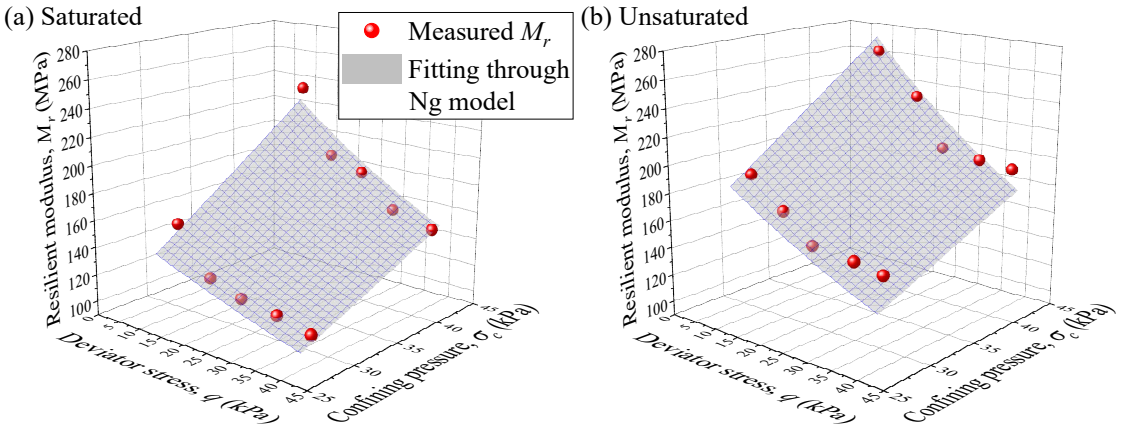

Fig. 8. Resilient modulus of U test under saturated and unsaturated condition.

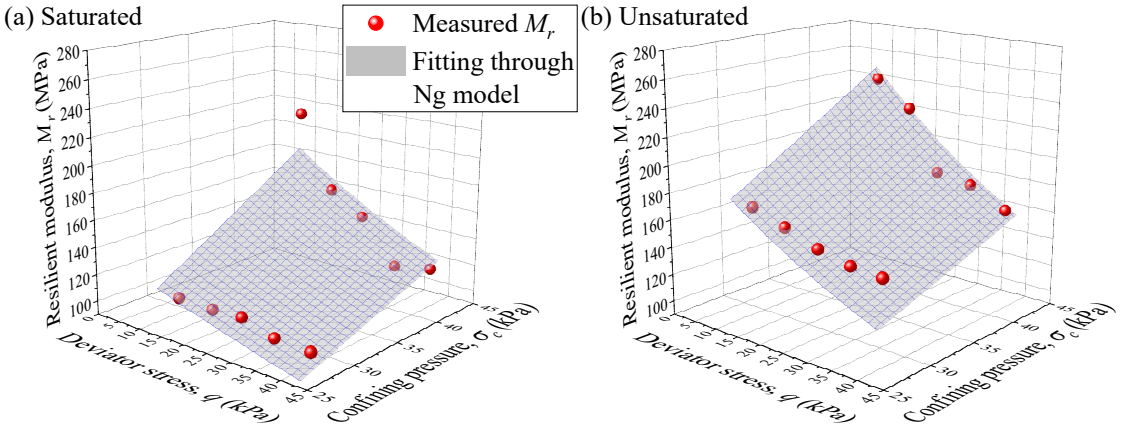

Fig. 9. Resilient modulus of UW test under saturated and unsaturated condition.

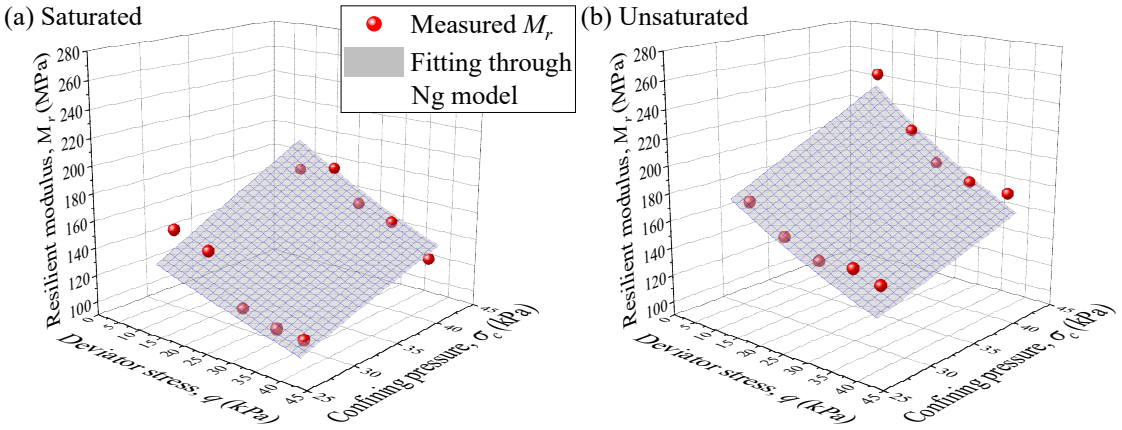

Fig. 10. Resilient modulus of FT test under saturated and unsaturated condition.

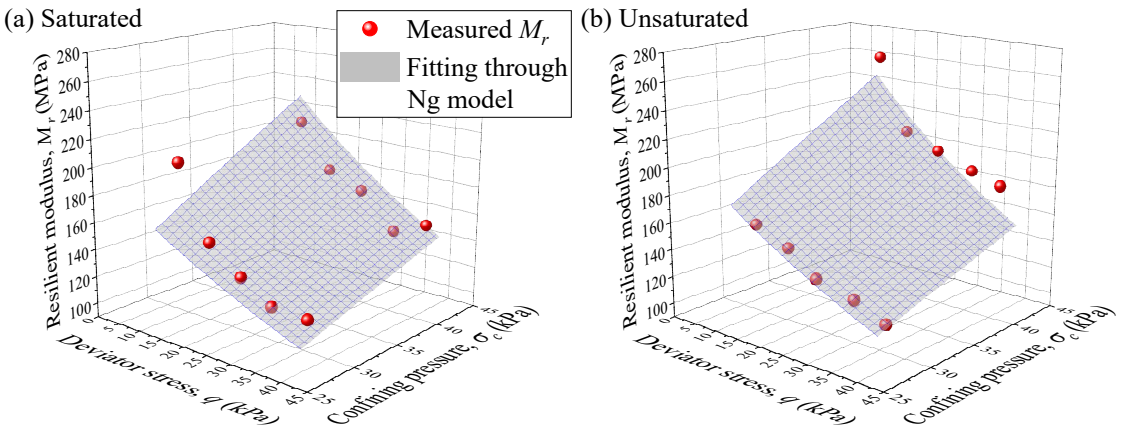

330

331 Fig. 11. Resilient modulus of FTW test under saturated and unsaturated condition.

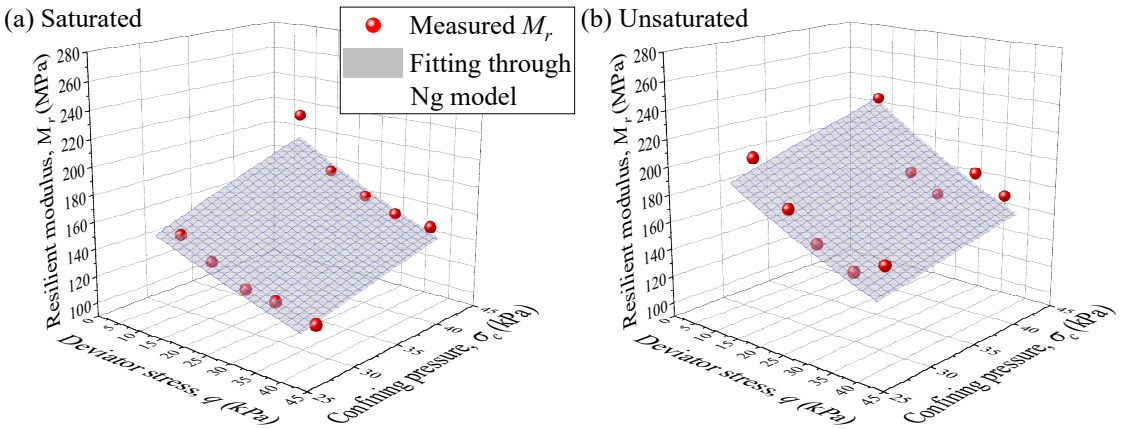

332

333 Fig. 12. Resilient modulus of FWT test under saturated and unsaturated condition.

334 Table 3. Regression analysis results through Ng model.

Test name	k_1	k_2	k_3	k_4	R^2
U	2.103	1.065	-4.843	2.740	0.949
UW	1.750	1.088	-4.916	3.639	0.905
FT	1.873	0.844	-4.111	2.474	0.910
FTW	2.328	0.823	-4.967	0.845	0.803
FWT	2.011	0.538	-3.382	1.766	0.805

335 *5.3 Effects of freeze-thaw action*

336 Freeze-thaw action decreases the M_r when other test conditions are the same as revealed by the com-

337 parison between U and FT tests or UW and FTW tests no matter under saturated or unsaturated

conditions. Another phenomenon worth to pointing out is all M_r surfaces in the freeze-thawed test are lower and flatter compared with those surfaces in the unfrozen test. This observation through geometry view could be described as when the σ_c increases the same amount in both unfrozen tests (U or UW) and freeze-thawed tests (FT or FTW), the M_r of the unfrozen specimen would increase more significantly. Besides, when q increases the same amount in both unfrozen tests (U or UW) and freeze-thawed tests (FT or FTW), the M_r of the unfrozen specimen would decrease more significantly. In other words, freeze-thaw also lowers the sensitivity of M_r to stress variables like q or σ_c. These findings indicate that only attribute thaw weakening to suddenly rising water content is not sufficient for modeling the M_r. Even without rising water content, freeze-thaw action could also degrade the stiffness of subgrade material. Thaw weakening is more like a synergistic effect between freeze-thaw and fluctuating water content. Past research (Lin et al., 2019b) observed that specimen height would increase, and the water would drain out of the specimen when water is transforming to ice in the freezing process due to the 9% volumetric expansion. Accordingly, with the melting of ice in thawing process, specimen height would decrease, and water would drain into the specimen. With the expansion and settled down of specimen, the soil particle skeleton structure is rearranged. It is reasonable to assume that the freeze-thaw process deteriorates the uniformity of particle skeleton structure and finally leads to worse mechanical properties. In fact, changes in soil structure of clay due to freeze-thaw has been investigated by some researchers. By X-ray μCT scanning, Starkloff et al. (2017) determined a reduction in macroporosity (>140 μm pore diameter), pore thickness, and their specific surface area for a silty clay loam and especially for a loamy sand after several feeeze-thaw cycles. Wang et al. (2018) observed close correlations between the physical property changes and the CTI, variation in CT image intensity, for clay before and after freeze-thaw cycles. Leuther and Schlüter (2021) found that frost action induced a consolidation of repacked soil clods, resulting in a systematic reduction in pore sizes and macropore connectivity by X-ray μCT. It is noted that a more detailed and explicit study on soil structure of sand before and after freeze-thaw or track of water migration during freeze-thaw process is necessary to support this assumption.

5.4 Effects of wheel loads

For unfrozen specimen, the wheel loads reduce M_r, as indicated in Figs. 8 and 9 (U test and UW test), partly due to the disturbance of soil particle skeleton structure uniformity caused by wheel loads. Whereas, the wheel loads after the freeze-thaw process elevate M_r a little, as illustrated in Figs. 10 and 11 (FT test and FTW test). In this case, the role of wheel loads for freeze-thawed soil is some kind of consolidation to help the specimen regain the uniformity of particle skeleton structure. On the other hand, wheel loads applied on a frozen specimen do not affect M_r greatly, as shown through the comparison between results from FT test and FWT test (see Figs. 10 and 12). A reasonable explanation for this phenomenon is that a frozen specimen has a much higher stiffness than a thawed specimen. Figs. 13 and 14 demonstrate the relationship between the loading number, N_c, and axial strain, ε_a, and Secant Young's modulus, E_s, during wheel loads process in FWT test and FTW test separately. It is noted that the Secant Young's modulus (E_s) in this study is defined as the ratio of cyclic deviator stress to the maximum axial strain, $(\varepsilon_a)_{max}$, during one loading cycle, which consists of recoverable axial strain, $(\varepsilon_a)_r$, and permanent axial strain, $(\varepsilon_a)_p$. The smallest axial strain during one loading cycle is defined as $(\varepsilon_a)_p$. It is obvious that a frozen specimen has a larger modulus than an unfrozen specimen when the degree of saturation is the same. To be specific, the stiffness of frozen saturated or unsaturated specimens is 6 or 3 times that of the thawed specimen. Within all frozen specimens, though saturated one has a much larger stiffness than unsaturated one as more ice is formed in the saturated specimen, axial strains in these two specimens are both at a very low level. Despite frost-susceptibility of the soil, freezing action significantly amplifies the stiffness of the specimen since ice has a much larger stiffness as compared with soils. Consequently, the axial strain of frozen specimen, no matter maximum axial strain, $(\varepsilon_a)_{max}$, or permanent axial strain, $(\varepsilon_a)_p$, will be a very small value compared with those of thawed specimen. An extremely low ε_a for saturated frozen specimen causes the variation in measured stiffness as the axial displacement transducer fluctuates when measuring such low value. Besides, by comparing Fig. 14 (a) and (b), the unsaturated specimen shows a larger E_s and smaller ε_a than those of the saturated specimen, which implies that matric suction strengthens the mechanical properties of a thawed specimen.

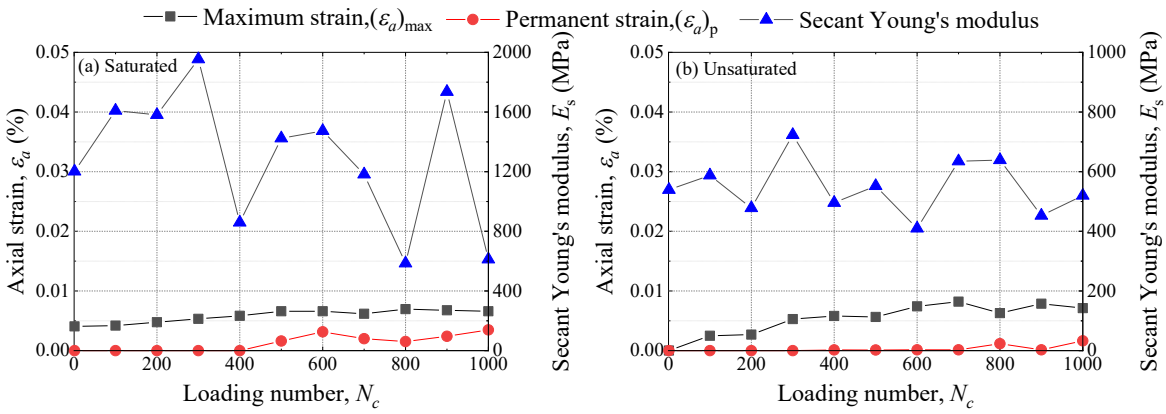

390

391 Fig. 13. Axial strain and Secant Young's modulus during wheel loads process in FWT test.

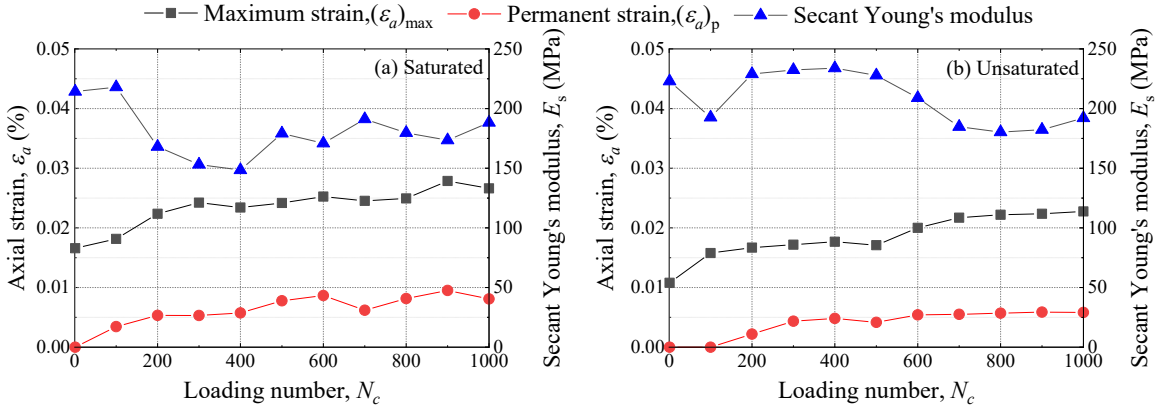

392

393 Fig. 14. Axial strain and Secant Young's modulus during wheel loads process in FTW test.

394 **6. Proposal of a modified climate model**

395 *6.1 Applicability of EICM*

396 As above mentioned, both freeze-thaw and rising water content have a negative influence on the resili-
397 ent modulus. In general, these two factors both contribute to the thaw weakening illustrated by compar-
398 ing M_r of unsaturated unfrozen (Fig. 8 (b)) and saturated freeze-thawed test (Fig. 10 (a)). This syner-
399 gistic effects of water content and freeze-thaw on M_r has a more complicated mechanism. By comparing
400 Fig. 8 and 10, decreasing amount of M_r is more significant in a saturated condition, which implies that
401 a decrease in M_r caused by freeze-thaw is strongly related to the water content before freezing. More
402 water contents exist in a specimen when the freeze-thaw action is applied, the M_r decreases more sig-
403 nificantly after a freeze-thaw action. It is reasonable to assume that the amount of ice formed during the

freezing period has a positive relationship with the change of particle skeleton structure and the decreasing amount of M_r.

Ng model uses the regression constants k_2, k_3, and k_4 to reflect the influence of bulk stress, θ, octahedral shear stress, τ_{oct}, and matric suction, ψ, on M_r separately. Since M_r increases with larger θ and ψ, k_2 and k_4 are positive values. Besides, as M_r decreases with larger τ_{oct}, k_3 is a negative value. As a result, a larger absolute value of k_2, k_3, and k_4 means a higher effect of θ, τ_{oct}, and ψ on M_r. As shown in Table 3, k_2, k_3, and k_4 of the FT test have smaller absolute values comparing with them in the U test, which is consistent with observations that freeze-thaw weakens the influence of θ, τ_{oct}, and ψ.

Regression analysis for FT and FTW tests through EICM is performed to check its applicability and validity. To extend this model into unsaturated conditions, F_{env} in Eq. (3) is added on the Ng model (Eq. (2)) in a similar way as shown in Eq. (7). As mentioned before, EICM estimates the reduction of M_r caused by freeze-thaw action with an adjustment factor, F_{env}. To examine whether this parameter could fully capture the climate effect, regression analysis is conducted with one variable, F_{env}, and four fixed parameters, k_1, k_2, k_3, and k_4. k_1 to k_4 are determined by regression analysis results of U and UW tests obtained by Ng model (Eq. (2)).

$$M_r = F_{env} \cdot k_1 p_a \left(\frac{\theta}{p_a}\right)^{k_2} \left(\frac{\tau_{oct}}{p_a} + 1\right)^{k_3} \left(\frac{\psi}{\sigma_{net}} + 1\right)^{k_4} \quad (7)$$

Table 4 lists the regression analysis results of FT and FTW tests through EICM model (Eq. (7)). A decreasing R^2 value compared with R^2 shown in Table 3 implies the conventional model cannot fully capture the climate effect. Structure in Eq. (7) indicates that k_2, k_3, and k_4 are not influenced by F_{env}, as EICM assumes the climate effect only raises or lowers the M_r surface but does not change the surface shape. However, as shown in Figs. 8 to 12, it is so obvious that this assumption is not consistent with test results in this study, that is climate effect not only raise or lower the M_r surface but also change the surface shape.

Table 4. Applicability of EICM and modified Ng models.

Test name	k_1	k_2	k_3	k_4	F_{env}	F_{clim}	R^2

U test	2.103	1.065	-4.843	2.740	—	—	0.949
FT test (EICM)	2.103	1.065	-4.843	2.740	0.897	—	0.872
FT test (Modified)	2.103	1.065	-4.843	2.740	—	0.885	0.901
UW test	1.750	1.088	-4.916	3.640	—	—	0.905
FTW test (EICM)	1.750	1.088	-4.916	3.640	0.680	—	0.506
FTW test (Modified)	1.750	1.088	-4.916	3.640	—	0.668	0.619

6.2 Modified Ng model

To overcome this drawback, this study assumes the climate effect could be expressed by an adjusting factor that decreases k_1, k_2, k_3, and k_4 with the same ratio. This assumption is quite reasonable as k_1, k_2, k_3, and k_4 all have a smaller absolute value by a similar degree when the specimen is subjected to freeze-thaw action, indicated by regression analysis results of U test and FT test in Table 3. Based on this assumption, Ng model (Eq. (2)) is modified by adding a new parameter, F_{clim}, into all regression parameters (k_1, k_2, k_3, and k_4), as shown in Eq. (8). Same as before, it is noted that only F_{clim} is variable and k_1 to k_4 are fixed as the value obtained through regression analysis results of U or UW test.

$$M_r = F_{clim} \cdot k_1 p_a \left(\frac{\theta}{p_a}\right)^{F_{clim} \cdot k_2} \left(\frac{\tau_{oct}}{p_a} + 1\right)^{F_{clim} \cdot k_3} \left(\frac{\psi}{\sigma_{net}} + 1\right)^{F_{clim} \cdot k_4} \quad (8)$$

Regression analysis results of FT and FTW tests shown in Table 4 proved that modified Ng model has a better performance and accuracy compared with EICM. Fig. 15 illustrates the fitting surface for FT test results through EICM and modified Ng model. It is obvious that fitting surface through modified Ng model better matches test results compared with fitting surface through EICM. Consequently, the assumption is validated that freeze-thaw action lowers the influence of stress variables like bulk stress, octahedral shear stress, and matric suction and decreases k_1, k_2, k_3, and k_4 with the same ratio. It is noted that R^2 value of tests with wheel loads process, UW and FTW tests, are all lower than R^2 of tests without wheel loads process, U and FT tests. As discussed before, wheel loads process presents a complicated effect on the mechanical properties of specimen when it is applied on a frozen, thawed, or unfrozen specimen. Such a complicated effect decreases the accuracy of all models. A further and comprehensive study on wheel loads, especially how does it affect pavement fatigue life, is necessary.

448 Furthermore, principal stress axis rotation induced by wheel loads also needs to be considered as it
449 greatly reduces pavement fatigue life (Ishikawa et al., 2019b; Lin et al., 2019c).

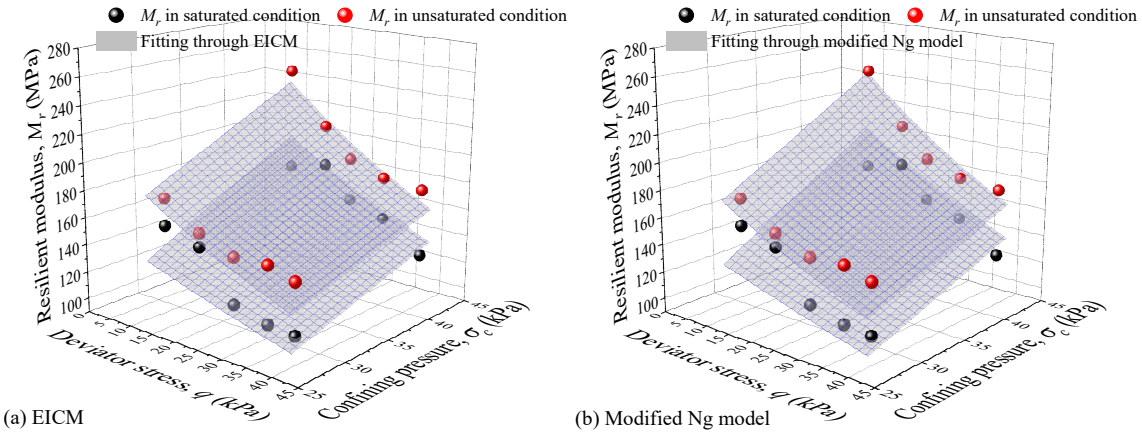

450

451 Fig. 15. Fitting surfaces of FT test results through (a) EICM (b) modified Ng model.

452 **7. Application to Japanese Pavement Design Guide**

453 *7.1 Fatigue life analysis of asphalt pavement*

454 To evaluate the climate effect on the degradation of subgrade layer, this chapter discusses the fatigue
455 life of the asphalt pavement in cold regions. Japanese design guide provides fatigue failure criteria to
456 calculate allowable number of equivalent 49-kN wheel loads against rutting (N_{fs}) and fatigue cracking
457 (N_{fa}), which are calculated by a theoretical design method (Asphalt Institute, 1982) using a simplified
458 three-layers model which consists of As layer, base layer, and subgrade layer as shown in Fig. 16. In
459 general, the Japanese pavement design guide assumes the elastic moduli of base layer (E_2) and subgrade
460 layers (E_3) are constant throughout a whole year. However, Ishikawa et al. (2019a) discussed the influ-
461 ences of the seasonality in E_2 on the fatigue life of the asphalt pavement in cold regions by considering
462 freeze-thaw action and seasonal fluctuation in water content through combining in-situ measured stiff-
463 ness and laboratory tested stiffness data. In this study, to capture the seasonality of the E_3 and its effect
464 on pavement fatigue life, E_2 is kept as a constant and E_3 varies considering freeze-thaw action and the
465 associated seasonal fluctuation in water content. Moreover, since E_3 does not have a significant effect
466 on the N_{fa} calculation model employed in the Japanese pavement design guide, only N_{fs} is calculated in
467 this study using Eq. (9) (Japan Road Association, 2006).

468 It is noted that the three-layers model shown in Fig. 16 is simplified from the five-layers model shown
469 in Fig. 5 by combining asphalt and stabilization into As layer and base and subbase into base layer.
470 Such simplification is recommended since this study focuses on the effect of the seasonality of the E_3
471 on pavement fatigue life, N_{fs}. Clear distinguishing between asphalt and stabilization or base and subbase
472 does not greatly affect the calculated N_{fs} with changing E_3. Besides, three-layers model helps achieve
473 consistency when performing case study since only asphalt, base, and subgrade layer are essential in
474 actual flexible pavement structure while stabilization and subbase layer are not always set (Fig. 17).

475 $$N_{fs} = \beta_{s1} \cdot \{1.365 \times 10^{-9} \cdot {\varepsilon_a}^{-4.477 \cdot \beta_{s2}}\} \quad (9)$$

476 where β_{s1}=2134 and β_{s2}=0.819 are the compensation coefficients for Asphalt Institute model based on
477 the actual situation of Japanese pavement; ε_a is the compressive strain on the top surface of the subgrade
478 layer under a design wheel load of 49 kN, which is greatly affected by E_3.

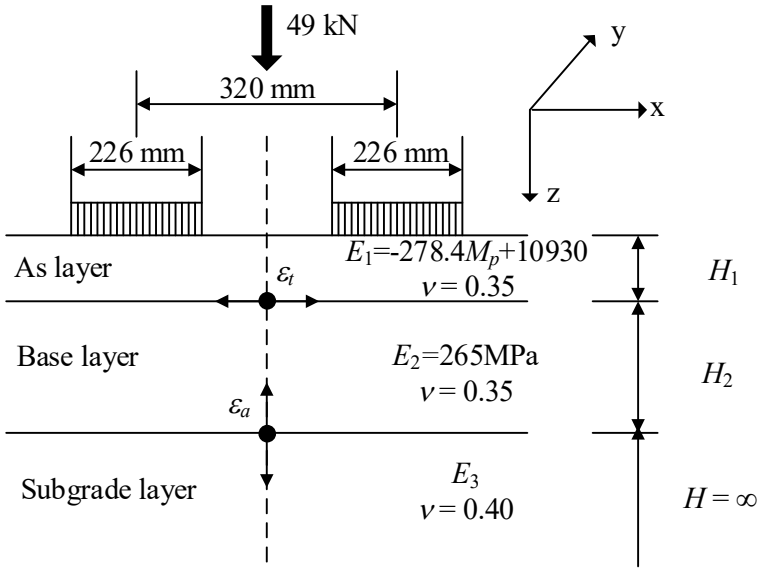

M_p: Monthly mean temperature of As layer.

479

480 Fig. 16. Cross section used in GAMES.

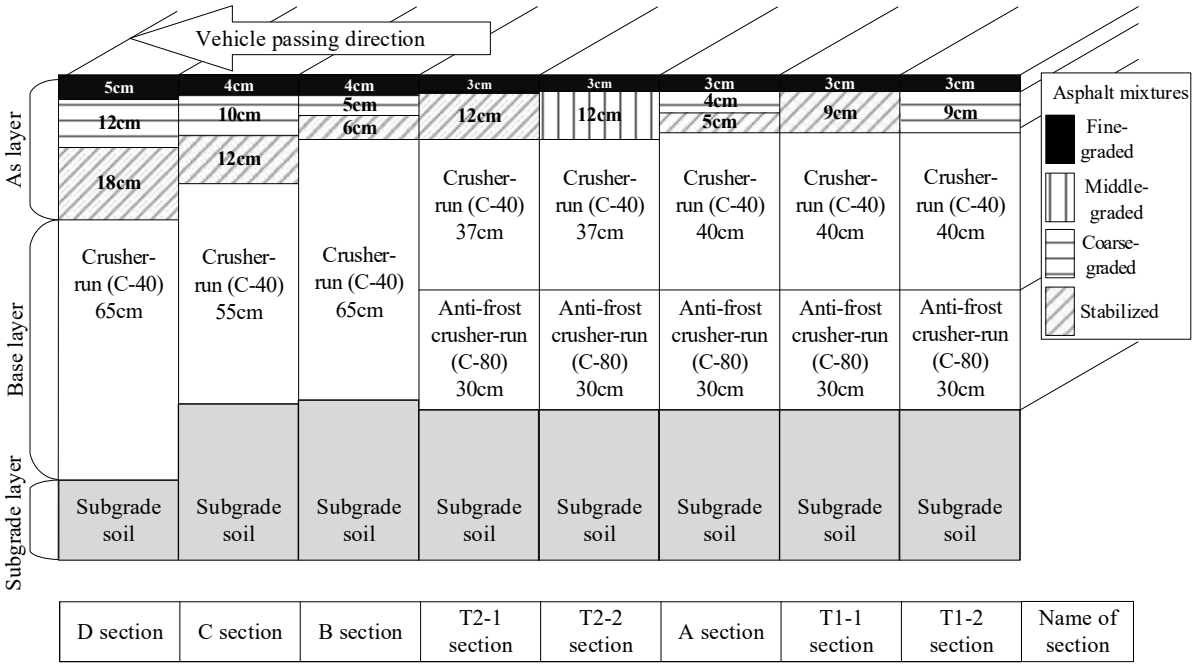

Fig. 17. Pavement structure models.

This study performed fatigue-life analysis against eight test pavement structures located at Hokkaido, Japan. Civil Engineering Research Institute for Cold Region (CERI) designed and constructed eight test pavements (Maruyama et al., 2006). Fig. 17 illustrates the structures and length of each test pavement. All eight pavement structures consist of asphalt mixture, base layer, and subgrade layer with multiple materials and thicknesses. Four types of asphalt mixtures are used in test pavement. Fine-graded asphalt mixture has a 0 - 13 mm gradation distribution. Middle-graded asphalt mixture has the same range of gradation distribution but more coarse aggregate. Coarse-graded and stabilized asphalt mixture have a 0 - 20 mm and 0 - 30 mm gradation distribution separately. Two types of base layer material are used as C-40, crusher-run with maximum 40 mm gradation distribution, and C-80, anti-frost crusher-run with maximum 80 mm gradation distribution. The asphalt mixtures, crusher-run materials, and subgrade soil in one section are simplified into the As layer, base layer, and subgrade layer separately in GAMES analysis (Fig. 16). Consequently, all eight sections could be simplified into three layers models with different layer thicknesses to estimate ε_a through GAMES analysis. Then, monthly fatigue life against rutting, $N_{fs,i}$, is calculated with monthly representative layer moduli. The total fatigue life against rutting, $N_{fs,d}$, is calculated through Eq. (10).

$$N_{fs,d} = 12/\sum_{i=1}^{12} \frac{1}{N_{fs,i}} \quad (10)$$

Stiffness of asphalt mixture (E_1) is determined through the following equations (Japan Road Association, 2006; Maruyama et al., 2008).

$$E_1 = -278.4M_p + 10930 \quad (11)$$

$$M_p = M_a\left[1 + \frac{2.54}{h+10.16}\right] - \frac{25.4}{9(h+10.16)} + \frac{10}{3} \quad (12)$$

where M_p is the monthly mean temperature of asphalt mixture at depth of h (℃); M_a is monthly mean air temperature (℃); h is the depth equals to one-third of the height of asphalt mixture (cm).

Constant stiffness of base layer (E_2) through the year is set as 265MPa referring to previous research (Maruyama et al., 2008).

When considering the climate effect, freeze-thaw action and seasonal fluctuation in water content, on the stiffness of subgrade layer, the monthly representative elastic moduli were divided into three types of seasonal E_3 values (E_3 for freezing season, thawing season, and regular season except for freezing and thawing seasons) for the simplicity of the fatigue life analysis. The E_3 value for freezing season is set as 200 MPa, according to the back analysis of FWD test results (Ishikawa et al., 2019a). Though Young's modulus of freezing unsaturated specimen is detected around 600 MPa as shown in Fig. 11, this test result was obtained under fully frozen status, which may be different from the in-situ condition that only top of subgrade layer is frozen during winter season. Consequently, a 200 MPa modulus from in-situ FWD test is treated as a more suitable value for the E_3 to represent whole subgrade layer during freezing season. In addition, this study assumes that when the average frost-penetration depth for the month gets into the subgrade layer regardless of deep or shallow, the E_3 increases due to freezing. Here, the average frost-penetration depth (z) was calculated by substituting the freezing index calculated from the daily mean air temperatures measured by AMeDAS (Automated Meteorological Data Acquisition System) into the modified Berggren formula (Aldrich Jr, 1956) shown below:

$$z = \alpha\sqrt{\frac{172800F}{(L/\lambda)_{eff}}} \quad (12)$$

where α is a correction coefficient; F is a freezing index which is the average air temperature during freezing season multiplied by its duration in days; $(L/\lambda)_{eff}$ is an effective ratio of L to λ; L is the latent heat of soil; λ is a thermal conductivity of the soil.

The E_3 value for the regular season is estimated by substituting the value of k_1, k_2, k_3, and k_4 into Ng model as shown in Eq. (13). The principal stress ratio is equal to 4 under 5 kPa confining pressure to determine bulk stress and octahedral shear stress. It is noted that this stress condition was selected so that M_r at normal season matches layer stiffness determined in previous research (Maruyama et al., 2008).

$$M_r = 2.103 \cdot p_a \left(\frac{\theta}{p_a}\right)^{1.065} \left(\frac{\tau_{oct}}{p_a} + 1\right)^{-4.843} \left(\frac{\psi}{\sigma_{net}} + 1\right)^{2.74} \quad (13)$$

The matric suction in subgrade layer is also necessary to estimate E_3. Ishikawa et al. (2012) performed long-term field measurements of frost-penetration depth, daily precipitation, and degree of saturation in each layer of the pavement. Fig. 18 illustrates the long-term field measured degree of saturation, S_r, of subgrade layer through a year. The subgrade material is a sandy soil, named Tomakomai soil, composed of 8% clay, 13% silt, 51% sand, 28% gravel. This study uses Toyoura sand to represent the subgrade layer since the mechanical and hydraulic properties of Tomakomai soil are under investigation. It is assumed that effective degree of saturation, S_e, would be same in Toyoura sand subgrade and Tomakomai soil subgrade under same climate condition. S_e of subgrade layer illustrated in Fig. 18 was calculated by using a residual degree of saturation (S_{rr}) of 25.67%, which was determined through the SWCC estimated with grain-size distribution of Tomakomai soil (Fredlund et al., 2002). Consequently, monthly average S_e is selected to determine matric suction of subgrade layer in each month through SWCC of Toyoura sand (Fig. 2), and monthly representative M_r is calculated by Eq. (13).

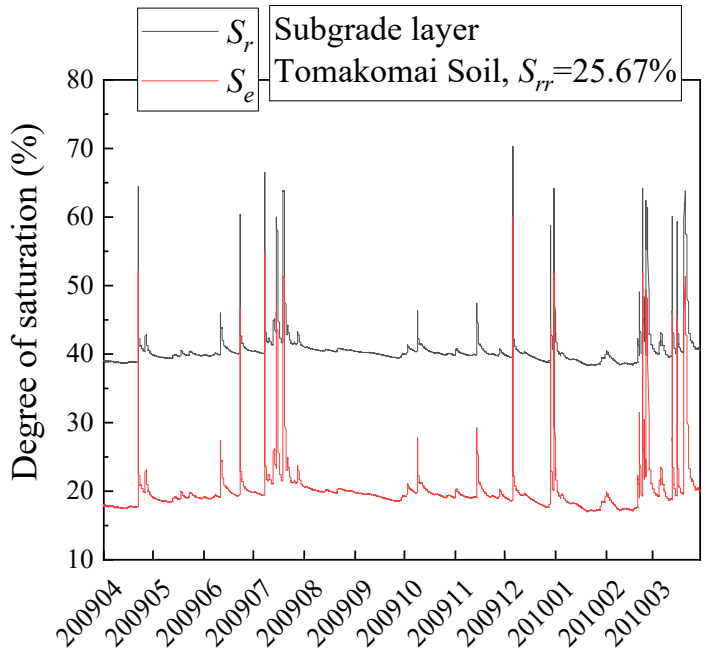

Fig. 18. Long-term field measured S_r of subgrade layer.

The E_3 value for thawing season is estimated by modified Ng model with considering climate effect, F_{clim}. By substituting F_{clim} and the value of k_1, k_2, k_3, and k_4 into Eq. (8), the M_r of the thawed season could be estimated as shown in Eq. (14) and (15). It is noted that matric suction used here corresponds to the highest water content during thawing season. In other words, E_3 value for thawing season stands for the worst situation, and the recovering period from thawing season to regular season is not considered in this paper. A furthermore comprehensive model is under developing to capture the recovering period.

$$M_r = F_{clim} \cdot 2.103 \cdot p_a \left(\frac{\theta}{p_a}\right)^{F_{clim} \cdot 1.065} \left(\frac{\tau_{oct}}{p_a} + 1\right)^{F_{clim} \cdot -4.843} \left(\frac{\psi}{\sigma_{net}} + 1\right)^{F_{clim} \cdot 2.74} \quad (14)$$

$$F_{clim} = 0.885 \quad (15)$$

Table 5. Monthly representative elastic moduli of subgrade layer, E_3.

		Jan	Feb	Mar	Apr	May	Jun	Jul	Aug	Sep	Oct	Nov	Dec
Original design guide		76	76	76	76	76	76	76	76	76	76	76	76
Water content fluctuation	10 Hz	77	75	61	76	76	71	69	76	76	76	76	75
	0.2 Hz	71	69	55	70	70	65	63	70	70	70	70	69
Climate effect	10 Hz	77	200	50	76	76	71	69	76	76	76	76	75

0.2 Hz	71	200	45	70	70	65	63	70	70	70	70	69

Consequently, Table 5 lists the estimated monthly representative E_3 through a year with consideration of climate effect under different loading frequencies. E_3 (f=0.2 Hz) are estimated with original MR test data, while E_3 (f=10 Hz) are estimated with converted MR test data through Eqs. (5) and (6). As the climate effect is a synergistic effect between water content fluctuation and freeze-thaw action, it is essential to check climate effect step by step. For this reason, monthly representative E_3 only considering water content fluctuation under different loading frequencies are also calculated through Eq. (13) and shown in Table 5. Besides, referring to previous research (Maruyama et al., 2008), a constant E_3 through the year is set as 76MPa and applied in the original design guide condition. Poisson's ratio of As layer, base layer, and subgrade layer are set as 0.35, 0.35, and 0.4 separately, which come from the design guide recommend value.

From Table 5, it is recognized that compared with the original design guide condition, E_3 drops at early spring (Mar) and summertime (Jun and Jul) when the water content fluctuation is considered since snowmelt water and the thawing of ice lenses at thawing season and heavy rainfall at summertime increases the water content in subgrade layer and finally decreases the stiffness. When freeze-thaw action is also considered, E_3 drops furthermore at Mar due to the thaw weakening and increases to 200 MPa at Feb due to the freezing action. Besides, moduli decrease with loading frequency.

7.2 Loading frequency effect on fatigue life of the pavement

To discuss the influence of loading frequency on fatigue life against rutting, E_3 (f=0.2 Hz) and E_3 (f=10 Hz) listed in Table 5 are used to calculate N_{fs} in all eight test pavement structures. Fig. 19 displays the N_{fs} with variant E_3 considering water content fluctuation (named as "N_{fs}-Water content fluctuation") and climate effect (named as "N_{fs}-Climate effect") under different loading frequencies. It is obvious that N_{fs} (f=10Hz) are always larger than N_{fs} (f=0.2Hz) no matter only consider water content fluctuation or synergistic climate effect on E_3. To clearly discuss the loading frequency effect on the fatigue life, the ratio of N_{fs} (R_{Nf}) for different pavement structures are also plotted in Fig. 18. The R_{Nf} considering loading frequency with water content fluctuation or climate effect is determined through dividing the N_{fs} (f=0.2Hz) by the N_{fs} (f=10Hz) when considering water content fluctuation or synergistic climate effect

on E_3. R_{Nf} in all pavement structures are around 0.861, which implies that fatigue life decreases about 13.9% when loading frequency lowers from 10Hz to 0.2Hz. Conclusively, converting E_3 (f=0.2Hz) to E_3 (f=10Hz) is necessary as loading frequency effect could not be ignored.

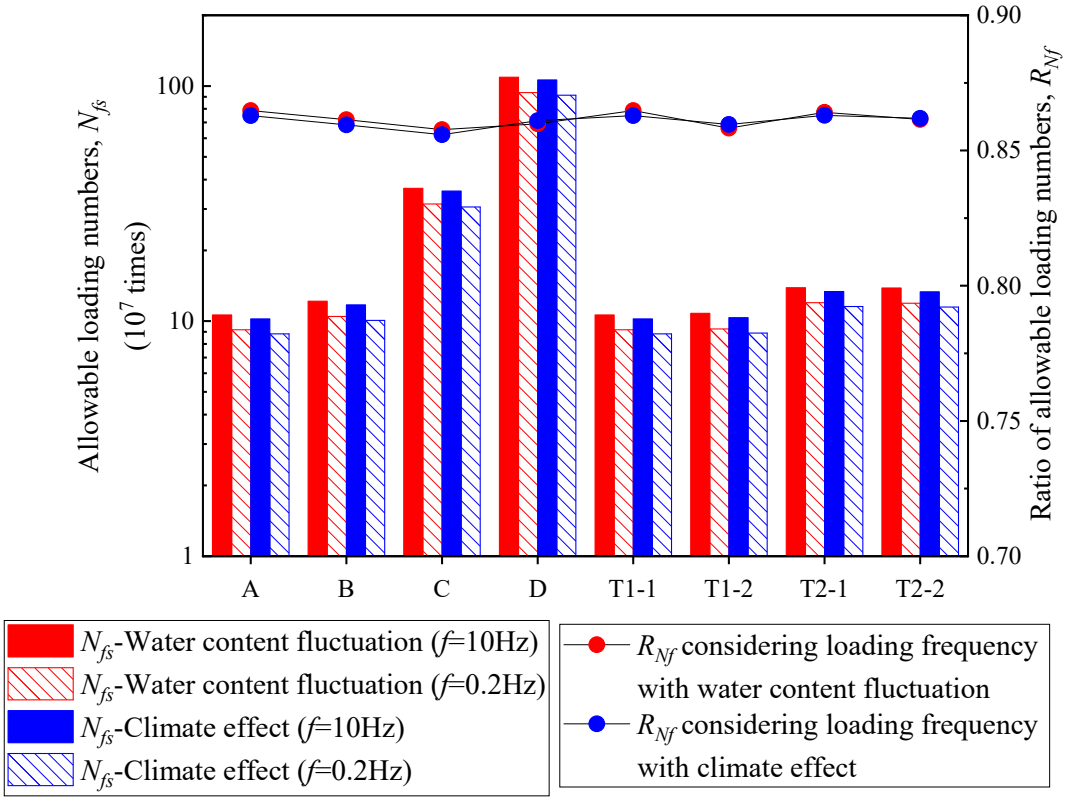

Fig. 19. Loading frequency effect on fatigue life against rutting.

7.3 Climate effect on fatigue life of the pavement

To discuss the climate effect, Fig. 20 displays the N_{fs}-Water content fluctuation and N_{fs}-Climate effect under 10Hz loading frequency. N_{fs} with constant E_3 of 76 MPa (named as "N_{fs}-Original") is also shown here. It is obvious that N_{fs}-Water content fluctuation is smaller than N_{fs}-Original but larger than N_{fs}-Climate effect, implies that reduced E_3 caused by sudden increasing water content decreases N_{fs} and freeze-thaw action decreases N_{fs} further as the reduced E_3 during thawing season has a stronger influence on the N_{fs} than the increasing E_3 during the freezing season. To clearly discuss the influence of water content fluctuation, freeze-thaw action, and climate effect on the fatigue life, R_{Nf} for different structures are also plotted in Fig. 20. The R_{Nf} considering water content fluctuation or climate effect are determined through dividing the N_{fs}-Water content fluctuation or N_{fs}-Climate effect by the N_{fs}-Original,

while the R_{Nf} considering freeze-thaw action is determined through dividing the N_{fs}-Climate effect by the N_{fs}-Water content fluctuation. All ratios are lower than 1, indicates that influence of water content fluctuation, freeze-thaw action, and climate effect on E_3 all decrease the fatigue life. R_{Nf} caused by water content, freeze-thaw action, and climate effect are around 0.938, 0.965, and 0.905 separately. In other words, the N_{fs} decreases 6.2% when changing E_3 caused by water content fluctuation is considered and it would further decrease 3.5% when effect of freeze-thaw action on E_3 is also considered. A synergistic climate effect on E_3 decreases N_{fs} about 9.5%.

These results suggest that for improving the applicability and validity of the current Japanese design standard, the introduction of the theoretical design method for pavement structures, which can take account of the effects of the freeze-thaw actions and the concurrent seasonal fluctuation in water content on the subgrade layer stiffness, is effective in the asphalt pavements for cold regions.

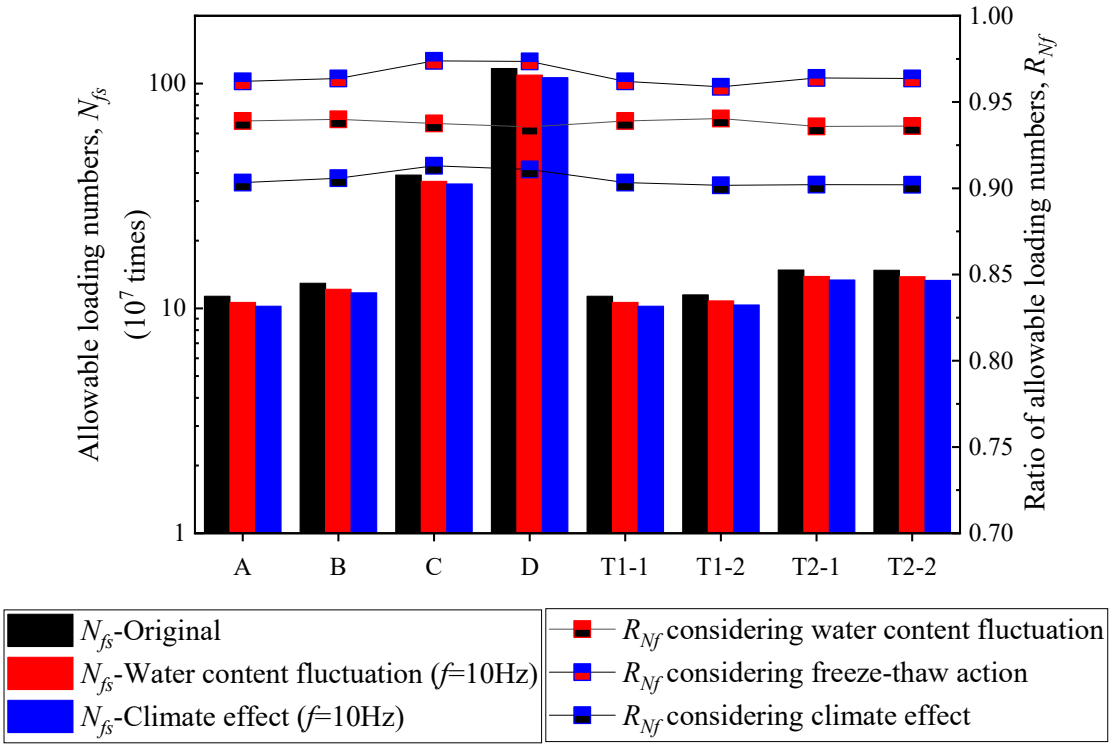

Fig. 20. Climate effect on fatigue life against rutting.

8. Conclusions

The following findings can be mainly obtained:

- Through performing a series of suction-controlled resilient modulus tests for a subgrade material with variant freeze-thaw, wheel loads, and water contents conditions, the effects of freeze-thaw actions and the concurrent seasonal fluctuations in water content (named as climate effect in this study) are examined and evaluated. As a consequence, climate effect degrades the resilient deformation characteristics of subgrade materials.
- Climate effect not only reduces the resilient modulus, but also weakens the influences of stress variables like bulk stress, octahedral shear stress, and matric suction on resilient modulus. Besides, the decreasing amount of resilient modulus caused by climate effect is more significant in a saturated condition, which implies that a synergistic effect of water content and freeze-thaw on the resilient modulus. The degradation in resilient modulus caused by freeze-thaw relates to the water content before the specimen is frozen. It is reasonable to assume that the amount of ice formed during the frozen period has a positive relationship with the change of particle skeleton structure uniformity and degradation of the mechanical properties of subgrade materials.
- A new parameter representing the climate effect, F_{clim}, is added into Ng model to quantitatively evaluate resilient modulus for the subgrade material under complex freeze-thaw, fluctuating water content, and variant stress states. Better performance compared with EICM proved the applicability and reliability of newly proposed modified Ng model.
- To modify current Japanese design guide by replacing constant subgrade layer moduli with a variant relating to water content fluctuation and freeze-thaw history, newly proposed modified Ng model, long-term measured in-situ subgrade layer water content, and laboratory obtained SWCC are used. Calculated fatigue life against rutting proves that both water content fluctuation and freeze-thaw action degrade stiffness of subgrade layer and finally decrease the fatigue life of asphalt pavements in cold regions. Accordingly, when developing a design method with high prediction accuracy for the asphalt pavements in cold regions, it is important to consider the change in the stiffness of subgrade layer caused by the climate conditions.

These findings indicate that a detailed understanding of the mechanical behavior of the subgrade during freeze-thaw is essential to develop a mathematical model for the mechanical response of the subgrade layer in cold regions and incorporate it into the theoretical design method for pavement structures. Further and more comprehensive studies including more unbound granular materials with various water contents are recommended to examine the validity, limitation of application, and so forth as these findings are obtained through limited experimental conditions.

Acknowledgements

This research was supported in part by Grant-in-Aid for Scientific Research (B) (20360206), (C) (15K06214), and (A) (16H02360) from Japan Society for the Promotion of Science (JSPS) KA-KENHI. The authors gratefully acknowledge research supports and invaluable comments come from Dr. Kimio Maruyama and the Civil Engineering Research Institute for Cold Region. The authors would also acknowledge the effort of Mr Ryosuke Aoki, former master student of Hokkaido University, who helped performed part of laboratory element tests. Support from China Scholarship Council is also highly acknowledged.

References

AASHTO, 2008. Mechanistic-empirical pavement design guide: a manual of practice, 2nd ed. American Association of State Highway and Transportation Officials (AASHTO), Washington DC.

AASHTO, 2003. Standard method of test for determining the resilient modulus of soils and aggregate materials: AASHTO designation T 307-99. American Association of State Highway and Transportation Officials, Washington D.C.

Aldrich Jr, H.P., 1956. Frost penetration below highway and airfield pavements. Highw. Res. Board Bull. 135, 124-149.

Aoki, R., Ishikawa, T., Tokoro, T., Lin, T., 2018. Evaluation method for resilient modulus of subgrade materials in cold regions. 58th Technical Report of the Annual Meeting of the JGS Hokkaido Branch, Sapporo; p. 23–30. [in Japanese]

Asphalt Institute, 1982. Research and Development of Asphalt Institute's Thickness Design Manual,

663 9th ed. Asphalt Institute, College Park Md.
664 Berg, R.L., Bigl, S.R.., Stark, J.A., Durell, G.D., 1996. Resilient modulus testing of materials from
665 Mn/Road: phase 1. https://doi.org/10.21949/1404573
666 Cary, C.E., Zapata, C.E., 2011. Resilient modulus for unsaturated unbound materials. Road Mater.
667 Pavement Des. 12 (3), 615–638. https://doi.org/10.1080/14680629.2011.9695263
668 Cary, C.E., Zapata, C.E., 2016. Pore water pressure response of soil subjected to dynamic loading un-
669 der saturated and unsaturated conditions. Int. J. Geomech. 16.
670 https://doi.org/10.1061/(ASCE)GM.1943-5622.0000642
671 Chen, C., Zhou, Z., Kong, L., Zhang, X., Yin, S., 2018. Undrained dynamic behaviour of peaty or-
672 ganic soil under long-term cyclic loading, Part I: Experimental investigation. Soil Dyn. Earthq.
673 Eng. 107, 279–291. https://doi.org/10.1016/j.soildyn.2018.01.012
674 Cole, D.M., Irwin, L.H., Johnson, T.C., 1981. Effect of Freezing and Thawing on Resilient Modulus
675 of a Granular Soil Exhibiting Nonlinear Behavior. Transp. Res. Rec. J. Transp. Res. Board 809,
676 19–26.
677 Fall, M., Tisot, J.P., Cisse, I.K., 1997. Undrained behaviour of compacted gravel lateritic soils from
678 western Senegal under monotonic and cyclic triaxial loading. Eng. Geol. 47, 71–87.
679 https://doi.org/10.1016/s0013-7952(96)00124-x
680 Fredlund, D.G., Morgenstern, N.R., 1977. Stress State Variables for Unsaturated Soils. J Geotech. Ge-
681 oenviron. 103 (5), 447–466.
682 Fredlund, D.G., Rahardjo, H., 1993. Soil Mechanics for Unsaturated Soils, Soil Mechanics for Un-
683 saturated Soils. John Wiley & Sons, Inc., Hoboken, NJ, USA.
684 https://doi.org/10.1002/9780470172759
685 Fredlund, D.G., Xing, A., 1994. Equations for the soil-water characteristic curve. Can. Geotech. J. 31
686 (4), 521–532. https://doi.org/10.1139/t94-061
687 Fredlund, M.D., Wilson, G.W., Fredlund, D.G., 2002. Use of the grain-size distribution for estimation
688 of the soil-water characteristic curve. Can. Geotech. J. 39 (5), 1103–1117.
689 https://doi.org/10.1139/t02-049
690 Guo, L., Wang, J., Cai, Y., Liu, H., Gao, Y., Sun, H., 2013. Undrained deformation behavior of

691 saturated soft clay under long-term cyclic loading. Soil Dyn. Earthq. Eng. 50, 28–37.
692 https://doi.org/10.1016/j.soildyn.2013.01.029
693 Han, Z., Vanapalli, S.K., 2016. State-of-the-art: Prediction of resilient modulus of unsaturated sub-
694 grade soils. Int. J. Geomech. 16 (4), 04015104. https://doi.org/10.1061/(ASCE)GM.1943-
695 5622.0000631
696 Ishikawa, T., Lin, T., Kawabata, S., Kameyama, S., Tokoro, T., 2019a. Effect evaluation of freeze-
697 thaw on resilient modulus of unsaturated granular base course material in pavement. Transp. Ge-
698 otech. 21, 100284. https://doi.org/10.1016/j.trgeo.2019.100284
699 Ishikawa, T., Lin, T., Yang, J., Tokoro, T., Tutumluer, E., 2019b. Application of the UIUC model for
700 predicting ballast settlement to unsaturated ballasts under moving wheel loads. Transp. Geotech.
701 18, 149-162. https://doi.org/10.1016/j.trgeo.2018.12.003
702 Ishikawa, T., Tokoro, T., Miura, S., 2016. Influence of freeze–thaw action on hydraulic behavior of
703 unsaturated volcanic coarse-grained soils. Soils Found. 56 (5), 790–804.
704 https://doi.org/10.1016/j.sandf.2016.08.005
705 Ishikawa, T., Zhang, Y., Tokoro, T., Miura, S., 2014. Medium-size triaxial apparatus for unsaturated
706 granular subbase course materials. Soils Found. 54 (1), 67–80.
707 https://doi.org/10.1016/j.sandf.2013.12.007
708 Ishikawa, T., Kawabata, S., Kameyama, S., Abe, R., Ono, T., 2012. Effects of freeze-thawing on me-
709 chanical behavior of granular base in cold regions. 10-12 September 2012. In: I Miura, H Yo-
710 shida, Abe, editors. Advances in transportation geotechnics II, Proc intern conf, Sapporo; p.
711 118–124.
712 Japan Road Association, 2006. Pavement design manual, Japan Road Association, Tokyo. [in Japa-
713 nese]
714 Japanese Geotechnical Society, 2009. Test Method for frost susceptibility of soils (JGS 0172-2003),
715 Standards of Japanese Geotechnical Society for Laboratory Soil Testing Methods; 2009. p. 45–
716 50. [in Japanese]
717 Johnson, T.C., Cole, D.M., Chamberlain, E.J., 1978. Influence of freezing and thawing on the resilient
718 properties of a silt soil beneath an asphalt concrete pavement. U.S. Cold Regions Research and

719 Engineering Laboratory, CRREL Report 78–23. http://hdl.handle.net/11681/9380
720 Jong, D.T., Bosscher, P.J., Benson, C.H., 1998. Field Assessment of Changes in Pavement Moduli
721 Caused by Freezing and Thawing. Transp. Res. Rec. J. Transp. Res. Board 1615 (1), 41–48.
722 https://doi.org/10.3141/1615-06
723 Kim, D.S., Kweon, G.-C., Lee, K.-H., 1997. Alternative Method of Determining Resilient Modulus of
724 Compacted Subgrade Soils Using Free-Free Resonant Column Test. Transp. Res. Rec. J. Transp.
725 Res. Board 1577 (1), 62–69. https://doi.org/10.3141/1577-08
726 Kishikawa, T., Otgonjargal, D., Kawaguchi, T., Nakamura, D., Yamashita, S., 2017. Influence of
727 freeze-thaw on stress propagation in the ground. Proc., 57th Technical Report of the Annual
728 Meeting of the JGS Hokkaido Branch, Kitami; p. 27–34. [in Japanese]
729 Khoury, N.N., Zaman, M.M., 2004. Correlation Between Resilient Modulus, Moisture Variation, and
730 Soil Suction for Subgrade Soils. Transp. Res. Rec. J. Transp. Res. Board 1874, 99–107.
731 https://doi.org/10.3141/1874-11
732 Leuther, F., Schlüter, S., 2021. Impact of freeze–thaw cycles on soil structure and soil hydraulic prop-
733 erties. Soil 7, 179-191. https://doi.org/10.5194/soil-7-179-2021
734 Liang, R.Y., Rabab'ah, S., Khasawneh, M., 2008. Predicting Moisture-Dependent Resilient Modulus
735 of Cohesive Soils Using Soil Suction Concept. J. Transp. Eng. 134 (1), 34–40.
736 https://doi.org/10.1061/(ASCE)0733-947X(2008)134:1(34)
737 Lin, B., Zhang, F., Feng, D., 2019. Long-term resilient behaviour of thawed saturated silty clay under
738 repeated cyclic loading: experimental evidence and evolution model. Road Mater. Pavement
739 Des. 20, 608–622. https://doi.org/10.1080/14680629.2017.1407819
740 Lin, T., Ishikawa, T., Aoki, R., 2019a. Resilient properties of unbound granular materials subjected to
741 freeze-thaw and wheel loads. Proc of 16th Asian Regional Conference on Soil Mechanics and
742 Geotechnical Engineering, Taipei.
743 Lin, T., Ishikawa, T., Tokoro, T., 2019b. Testing method for resilient properties of unsaturated un-
744 bound granular materials subjected to freeze-thaw action. Japanese Geotech. Soc. Spec. Publ. 7
745 (2), 576–581. https://doi.org/10.3208/jgssp.v07.089
746 Lin, T., Ishikawa, T., Luo, B., 2019c. Applicability of Modified University of Illinois at Urbana–

747 Champaign Model for Unbound Aggregate Material with Different Water Content, Transp. Res.
748 Rec. 2673 (3), 439-449. https://doi.org/10.1177/0361198119827530
749 Maina, J.W., Matsui, K., 2004. Developing Software for Elastic Analysis of Pavement Structure Re-
750 sponses to Vertical and Horizontal Surface Loadings. Transp. Res. Rec. J. Transp. Res. Board
751 1896 (1), 107–118. https://doi.org/10.3141/1896-11
752 Maruyama, K., Tako, J., Kasahara, A., 2008. Fatigue failure life prediction method of asphalt pave-
753 ment. J. JSCE. E 64 (3), 416–426. [in Japanese] https://doi.org/10.2208/jsceje.64.416
754 Maruyama, K., Tako, J., Kasahara, A., 2006. Long-term performance of asphalt pavements at bibi
755 new test road. J. JSCE. E 62 (3), 519–530. [in Japanese] https://doi.org/10.2208/jsceje.62.519
756 NCHRP, 2004. Guide for mechanistic-empirical design of new and rehabilitated pavement structures.
757 National Cooperative Highway Research Program 1-37 A.
758 Ng, C.W.W., Zhou, C., Yuan, Q., Xu, J., 2013. Resilient modulus of unsaturated subgrade soil: exper-
759 imental and theoretical investigations. Can. Geotech. J. 50 (2), 223–232.
760 https://doi.org/10.1139/cgj-2012-0052
761 Seed, H.B., CHAN, C.K., Monismith, C.L., 1955. Effects of repeated loading on the strength and de-
762 formation of compacted clay. Highw. Res. Board Proc. 34, 541-558.
763 Simonsen, E., Isacsson, U., 2001. Soil behavior during freezing and thawing using variable and con-
764 stant confining pressure triaxial tests. Can. Geotech. J. 38 (4), 863–875.
765 https://doi.org/10.1139/t01-007
766 Simonsen, E., Isacsson, U., 1999. Thaw weakening of pavement structures in cold regions. Cold Reg.
767 Sci. Technol. 29 (2), 135–151. https://doi.org/10.1016/S0165-232X(99)00020-8
768 Simonsen, E., Janoo, V.C., Isacsson, U., 2002. Resilient Properties of Unbound Road Materials dur-
769 ing Seasonal Frost Conditions. J. Cold Reg. Eng. 16 (1), 28–50.
770 https://doi.org/10.1061/(ASCE)0887-381X(2002)16:1(28)
771 Starkloff, T., Larsbo, M., Stolte, J., Hessel, R., and Ritsema, C., 2017. Quantifying the impact of a
772 succession of freezing-thawing cycles on the pore network of a silty clay loam and a loamy sand
773 topsoil using X-ray tomography. Catena, 156, 365–374. https://doi.org/10.1016/j.ca-
774 tena.2017.04.026

775 Wang, S., Yang, P., Yang, Z., 2018. Characterization of freeze–thaw effects within clay by 3D X-ray
776 Computed Tomography. Cold Reg. Sci. Technol. 148, 13-21. https://doi.org/10.1016/j.coldre-
777 gions.2018.01.001
778 Yang, S.-R., Huang, W.-H., Tai, Y.-T., 2005. Variation of Resilient Modulus with Soil Suction for
779 Compacted Subgrade Soils. Transp. Res. Rec. J. Transp. Res. Board 1913, 99–106.
780 https://doi.org/10.1177/0361198105191300110